CHALMERS
UNIVERSITY OF TECHNOLOGY

A PDE Model Simplification Framework for All-Solid-State Batteries

Citation for the original published paper (version of record):
Li, Y., Wik, T., Huang, Y. et al (2022). A PDE Model Simplification Framework for All-Solid-State Batteries. American Control Conference, 2022-June: 1775-1781.
http://dx.doi.org/10.23919/ACC53348.2022.9867316

(article starts on next page)

2022 American Control Conference (ACC)
Atlanta, USA, June 8-10, 2022

A PDE Model Simplification Framework for All-Solid-State Batteries

Yang Li, Torsten Wik, Yicun Huang, and Changfu Zou

Abstract— **All-solid-state batteries (ASSBs) have attracted immense attention due to their superior thermal stability, improved power and energy densities, and prolonged cycle life. Their practical applications require accurate and computationally efficient models for the design and implementation of many onboard management algorithms, so that the safety, health, and cycling performance of ASSBs can be optimized under a wide range of operating conditions. A control-oriented modeling framework is thus established in this work by systematically simplifying a partial differential equation (PDE) based model of the ASSBs developed from underlying electrochemical principles. Compared to the original PDE model, the reduced-order models obtained with the proposed framework demonstrates high fidelity at significantly improved computational efficiency.**

I. Introduction

All-solid-state batteries (ASSBs) have received increasing research attention in the last decade to overcome the problems plagued by conventional lithium-ion (Li-ion) batteries regarding safety and longevity [1]. In ASSBs, the organic liquid or polymer electrolytes in conventional Li-ion batteries are replaced with new types of electrolytes in a solid form. The solid electrolytes are non-flammable and highly thermally resistive, which prevents the problems of internal short circuit and electrolyte leakage. In addition, the solid-state electrolytes may also have better compatibility with Li metal anodes by providing a mechanical barrier to dendrite formation [2]. Also, the better adaptability to high-voltage cathode materials and Li metal anodes will greatly increase the energy density. When the technology has matured, such batteries are believed to get the merits of longer life, ensured safety, higher power and energy densities, and they are also believed to allow more flexible packing, making them suitable for more applications [3].

Although there have been significant material and structural breakthroughs in ASSBs, the battery system requires to be properly monitored and controlled during practical operation to fulfill the expectation of its longevity and high performance. Specifically, the information on internal battery states can be used for establishing charging/discharging strategies to balance the requirements of high safety, long service life, and fast load response. A suitable ASSB model with high fidelity and low computational burden is essential for online model-based management algorithms. A general and simple approach to battery modeling is to use equivalent circuit models. These have the advantage of ready-to-use implementations in well-accepted circuit simulation and control system design software packages. Conventionally obtained from system identification, the parametric values of such empirical models need to be adjusted regularly to fit the measurement data at different operating points. However, this approach to battery modeling has limited applicability for wider operating ranges and long-term battery performance prediction under the ever-changing system dynamics. Neither can degradation and internal safety be properly addressed due to the lack of insights regarding electrochemical dynamics.

For these reasons, much research has recently been devoted to investigating physics-based models with the capability of describing the internal electrochemical behaviors of ASSBs. Most of the existing methods have been established for conventional Li-ion batteries [4]–[6]. However, there have also been some initial attempts to mathematically model the dynamics of an ASSB. For example, Becker *et al.* [7] presented a model for ASSBs that takes into account the detailed ion transport in the solid solutions of crystalline metal oxides. Danilov *et al.* [8] developed an isothermal ASSB model that considers the imperfect dissociation of the ions in the electrolyte. This model consists of two partial differential equations (PDEs) that describe the diffusion processes in the solid electrolyte and in the positive electrode, respectively. The model in [8] has recently been improved and validated in [9] by considering the concentration-dependent diffusion coefficient. A battery state estimation method has been developed recently based on this model [10], where the PDEs are solved using the finite difference method. Resulting from the discretization, an ordinary differential equation (ODE) based battery model of high dimensionality was obtained. Because of the high order, the model is expensive to solve, which hinders the implementation of the designed estimator in many online applications. Model reduction methodologies have therefore recently been investigated for ASSBs, for control system design and implementation. For example, in [11], a PDE ASSB model was reduced using a combination of Padé approximation and polynomial profile approximation, and the computational burden was effectively reduced with high fidelity, allowing online operation [12]. However, the method fails to consider various practical limitations that can considerably reduce the applicability at high current rates, including the concentration-dependent diffusion and ionic migration behavior in the positive electrode.

In the present investigation, we propose a reduced-order modeling framework for ASSBs. Model simplification is systematically conducted using partial fraction expansion and moment matching, and the effect of concentration-dependent diffusion is addressed. The simplified models are benchmarked with a high-fidelity PDE model that has been

All authors are with the Department of Electrical Engineering, Chalmers University of Technology, Gothenburg, Sweden. yangli@ieee.org; tw@chalmers.se; yicun@chalmers.se; changfu.zou@chalmers.se

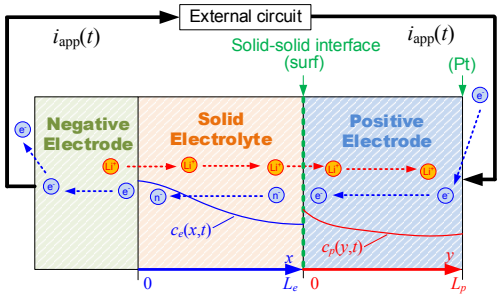

Fig. 1. Schematic of an ASSB cell during discharging.

experimentally validated under various current rates in the literature [13], and the results show the superiority of the proposed method to existing ones.

II. Overview of a PDE Model of ASSBs

This section presents an overview of a high-fidelity PDE model of the ASSBs under investigation [13]. The purpose is to provide fundamental background of the model structure and relevant equations for the development of the model simplification framework in latter sections.

A. System Description

The schematic of the one-dimensional model of a typical ASSB cell is shown in Fig. 1. The cell is divided into three physical domains along the horizontal axis, including porous positive electrode (e.g., $LiCoO_2$), negative electrode (e.g., metallic Li foil), and the solid electrolyte in between. The inner and the outer physical boundaries of the positive electrode domain are denoted by $y = 0$ and $y = L_p$, respectively, where L_p is the width of the positive electrode. The two boundaries of the solid electrolyte domain are denoted by $x = 0$ and $x = L_e$, respectively, with L_e being the width of the solid electrolyte. The Li concentration in the negative electrode is assumed to be a constant. This is different from conventional Li-ion batteries in which the porous electrodes are immersed in liquid or polymer electrolyte. The Li species will transport from the negative electrode to the positive electrode via the solid electrolyte by means of diffusion and migration during the discharge process, and a reverse process occurs when the battery is being charged.

B. Diffusion in the Solid Electrolyte

In the solid electrolyte, the mobile Li ions exist in equilibrium with the immobile Li ions. The immobile Li ions undergo an ionization reaction to generate the mobile Li ions and uncompensated negative charges (n^-) during the charge process, and a reverse reaction occurs during discharging. Under the electroneutrality condition and by ignoring the charge carrier generation effects, the diffusion and migration of the mobile Li ions can be described by

$$\frac{\partial c_e(x,t)}{\partial t} = D_e^{\text{eff}} \frac{\partial^2 c_e(x,t)}{\partial x^2} \tag{1a}$$

where c_e is the concentration of the mobile Li ions in the solid electrolyte, $D_e^{\text{eff}} := 2D_e^+ D_e^- / (D_e^+ + D_e^-)$ is the effective binary diffusion coefficient in the electrolyte, D_e^+ and D_e^- are the diffusion coefficients of the mobile Li ions and the uncompensated negative charges in the electrolyte, respectively. According to [13], the electrolyte concentrations do not vary significantly during cycling, and thus D_e^+ and D_e^- are considered constant. The boundary and the initial conditions of (1) are given by

$$D_e^+ \frac{\partial c_e(x,t)}{\partial x}\bigg|_{x=0} = D_e^+ \frac{\partial c_e(x,t)}{\partial x}\bigg|_{x=L_e} = \frac{i_{\text{app}}(t)}{2F} \tag{1b}$$

$$c_e(x, t=0) = c_{e0} = \delta c_0 \tag{1c}$$

where F is the Faraday constant and i_{app} is the applied current density defined as positive during charging. In addition, c_{e0} and c_0 represent the initial concentration of the mobile Li ions and the total Li ions in the electrolyte, respectively, and δ is the fraction of Li ions in the mobile states under the equilibrium condition.

C. Mass-Transfer Overpotential of the Solid Electrolyte

Electromigration and diffusion in the solid electrolyte induce the mass-transfer overpotential η_e^{mt} expressed by

$$\eta_e^{\text{mt}}(t) = \frac{RT}{F} \ln\left(\frac{c_e(L_e,t)}{c_e(0,t)}\right) - \int_0^{L_e} E_e(x,t)dx \tag{2}$$

where R is the universal gas constant, T is the cell temperature, and E_e is the electric field in the electrolyte, i.e.,

$$E_e(x,t) = \frac{RT}{F}\frac{1}{c_e(x,t)} \times \left[\frac{-i_{\text{app}}(t)}{2FD_e^+} + \frac{D_e^+ - D_e^-}{D_e^+ + D_e^-}\left(\frac{\partial c_e(x,t)}{\partial x} - \frac{i_{\text{app}}(t)}{2FD_e^+}\right)\right]. \tag{3}$$

D. Concentration-Dependent Diffusion in the Positive Electrode

Assuming the rate of phase transition has ignorable impacts on system performance, the diffusion of the Li ions in the positive electrode is governed by

$$\frac{\partial c_p(y,t)}{\partial t} = \frac{\partial}{\partial y}\left(D_p^{\text{eff}} \frac{\partial c_p(y,t)}{\partial y}\right) \tag{4a}$$

with the boundary and initial conditions

$$D_p^+ \frac{\partial c_p(y,t)}{\partial y}\bigg|_{y=0} = -D_p^- \frac{\partial c_p(y,t)}{\partial y}\bigg|_{y=L_p} = \frac{i_{\text{app}}(t)}{2F} \tag{4b}$$

$$c_p(y, t=0) = c_{p0} \tag{4c}$$

where c_p is the concentration of the Li ions in the positive electrode, $D_p^{\text{eff}} := 2D_p^+ D_p^- / (D_p^+ + D_p^-)$ is the effective binary diffusion coefficient in the positive electrode, and D_p^+ and D_p^- are the diffusion coefficients of the Li ions and the electrons in the positive electrode, respectively. In contrast to D_e^+ and D_e^-, both D_p^+ and D_p^- are considered concentration-dependent, according to $D_p^+(c_p) = f_{D+}(c_p)$ and $D_p^-(c_p) = f_{D-}(c_p)$.

The state-of-charge (SOC) of the ASSB is determined by the volumed-average Li-ion concentration c_p^{avg}, i.e.,

$$\text{SOC}(t) = \frac{c_p^{100\%} - c_p^{\text{avg}}(t)}{c_p^{100\%} - c_p^{0\%}} = \frac{c_p^{100\%} - \frac{1}{L_p}\int_0^{L_p} c_p(y,t)dy}{c_p^{100\%} - c_p^{0\%}} \tag{5}$$

where $c_p^{100\%}$ and $c_p^{0\%}$ are the Li-ion concentrations corresponding to SOC $= 100\%$ and SOC $= 0\%$, respectively.

E. Equilibrium Potential and Mass-Transfer Overpotential of the Positive Electrode

The Li-ion concentrations $c_p(0,t)$ and $c_p(L_p,t)$ at the two boundaries of the positive electrode are in the interest of the investigation. This is because the thermodynamic equilibrium potential U^{eq} and the overpotential η_p^{mt} due to the mass transfer in the electrode are solely determined by $c_p(0,t)$ and $c_p(L_p,t)$, i.e.,

$$U^{\text{eq}}(t) = h_1(c_p(0,t)) \tag{6}$$

$$\eta_p^{\text{mt}}(t) = \frac{RT}{F}\ln\left(\frac{c_p(L_p,t)}{c_p(0,t)}\right) - \int_0^{L_p} E_p(y,t)dy \tag{7}$$

where the electric field E_p is similar to E_e, as given in (3), and $h_1(\cdot)$ is a nonlinear function determined by the materials of the positive electrode.

F. Charge-Transfer Overpotentials and Terminal Voltage

The intercalation/de-intercalation reaction kinetics are described by the Butler-Volmer equation. The charge-transfer coefficients for both electrodes can be considered to be 0.5 [13], which gives the following expressions of the charge-transfer overpotential for both electrodes

$$\eta_p^{\text{ct}}(t) = \frac{2RT}{F}\sinh^{-1}\left(\frac{i_{\text{app}}(t)}{2i_{0,p}(t)}\right) \tag{8a}$$

$$\eta_n^{\text{ct}}(t) = -\frac{2RT}{F}\sinh^{-1}\left(\frac{i_{\text{app}}(t)}{2i_{0,n}}\right) \tag{8b}$$

where i_0 represents the average exchange current density of the intercalation defined under equilibrium conditions, i.e.,

$$i_{0,p}(t) = Fk_{0,p}\sqrt{c_{e0}c_p^{\text{avg}}(t)(c_p^{\max} - c_p^{\text{avg}}(t))} \tag{9a}$$

$$i_{0,n} = Fk_{0,n}\sqrt{c_{e0}c_n^{\text{avg}}} \tag{9b}$$

where $c_p^{\max}$ is the theoretical maximum concentration in the positive electrode and c_n^{avg} is the average concentration of the negative electrode.

The ASSB voltage is the sum of the equilibrium potential of the positive electrode and the overpotentials, i.e.,

$$V_{\text{bat}}(t) = U^{\text{eq}}(t) + \eta_p^{\text{mt}}(t) + \eta_e^{\text{mt}}(t) + \eta_p^{\text{ct}}(t) - \eta_n^{\text{ct}}(t). \tag{10}$$

III. A Model Order Reduction Framework

A. Simplified Solid-Electrolyte Diffusion Equation

First, we notice the general form of the Laplace transform of the solution to (1a) is

$$c_e(x,s) = A\sinh\left(\sqrt{s}x/\alpha\right) + B\cosh\left(\sqrt{s}x/\alpha\right) \tag{11}$$

where A and B are two coefficients and $\alpha = \sqrt{D_e^{\text{eff}}}$. The gradient of (11) is

$$\frac{\partial c_e(x,s)}{\partial x} = \frac{A\sqrt{s}}{\alpha}\cosh\left(\frac{\sqrt{s}x}{\alpha}\right) + \frac{B\sqrt{s}}{\alpha}\sinh\left(\frac{\sqrt{s}x}{\alpha}\right) \tag{12}$$

Next, defining $t_e^+ := D_e^+/(D_e^+ + D_e^-)$ as the transference number of the electrolyte and $t_e^- = 1 - t_e^+$, the boundary conditions (1b) can be rewritten in the complex frequency domain by

$$D_e^{\text{eff}}\frac{\partial c_e(x,s)}{\partial x}\bigg|_{x=0} = D_e^{\text{eff}}\frac{\partial c_e(x,s)}{\partial x}\bigg|_{x=L_e} = \frac{t_e^-}{F}i_{\text{app}}(s). \tag{13}$$

Using (12) and (13), one can solve for the coefficients A and B, both of which are proportional to the current density i_{app}. Substituting the resulting expressions of A and B into (11) yields the transfer function between c_e and i_{app}:

$$\frac{c_e(x,s)}{i_{\text{app}}(s)} = -\frac{t_e^-\tau_e}{2FL_e}\frac{1}{\frac{1}{2}\sqrt{\tau_e s}}\frac{\sinh\left(\left(\frac{2x}{L_e} - 1\right)\cdot\frac{1}{2}\sqrt{\tau_e s}\right)}{\cosh\left(\frac{1}{2}\sqrt{\tau_e s}\right)} \tag{14}$$

where $\tau_e = L_e^2/D_e^{\text{eff}}$ is the time constant of the electrolyte diffusion process.

Note that (14) has an anti-symmetrical property about the middle point $x = L_e/2$ of the solid-electrolyte domain. As seen in (2), we are particularly interested in the electrolyte concentrations at the domain boundaries. Hence, denoting $c_e^{\text{surf}}(t) := c_e(L_e,t)$ and using (14), the following transcendental transfer function at $x = L_e$ can be obtained,

$$\frac{c_e^{\text{surf}}(s)}{i_{\text{app}}(s)} = -\frac{t_e^-\tau_e}{2FL_e}G_e(s) \tag{15}$$

where

$$G_e(s) = \frac{\tanh\left(\frac{1}{2}\sqrt{\tau_e s}\right)}{\frac{1}{2}\sqrt{\tau_e s}} \tag{16}$$

For the purpose of control system design, a low-order rational transfer function describing a practically realizable system is needed. Since all singularities of $G_e(s)$ are of first order, corresponding to poles on the negative real axis, and can therefore be approximated by a series of first order transfer functions, i.e.,

$$G_e(s) \approx P_e(s) = \sum_{i=1}^{N_e}\frac{b_{e,i}}{\tau_e s + a_{e,i}} \tag{17}$$

where N_e is the order of the approximation and $a_{e,i}$ and $b_{e,i}$ are the PFE coefficients for the electrolyte diffusion equation. With this approximation, (17) can be realized as

$$\frac{d\tilde{c}_{e,i}(t)}{dt} = -\frac{a_{e,i}}{\tau_e}\tilde{c}_{e,i}(t) - \frac{b_{e,i}t_e^-}{2FL_e}i_{\text{app}}(t) \quad \forall i \in \mathcal{N}_e \tag{18a}$$

$$c_e^{\text{surf}}(t) = c_{e0} + \sum_{i=1}^{N_e}\tilde{c}_{e,i}(t) \tag{18b}$$

where $\mathcal{N}_e = \{1, 2, \cdots, N_e\}$.

To determine the $2N_e$ PFE coefficients $a_{e,i}$ and $b_{e,i}$, $i \in \mathcal{N}_e$, moment matching (MM) is adopted here [14]. Specifically, we set $P_e(0) = G_e(0)$ and do the same for the

first $(2N_e-1)$ derivatives of $P_e(0)=G_e(0)$ for $s=0$, establishing $2N_e$ equations that uniquely determines the values of all coefficients $a_{e,i}$ and $b_{e,i}$. The results up to $N_e=3$ are provided in Table I.

TABLE I
PFE COEFFICIENTS FOR THE ELECTROLYTE DIFFUSION EQUATION

	$a_{e,1}$	$b_{e,1}$	$a_{e,2}$	$b_{e,2}$	$a_{e,3}$	$b_{e,3}$
$N_e=1$	12	12	–	–	–	–
$N_e=2$	9.88	8.02	170.12	31.98	–	–
$N_e=3$	9.87	8	91.23	9.01	738.9	66.99

B. Simplified Positive Electrode Diffusion Equation Under Constant Diffusion Coefficients

Similar to the solid electrolyte, the boundary conditions of the diffusion equation (4) of the positive electrode can be rewritten as

$$D_p^{\text{eff}}\frac{\partial c_p(y,t)}{\partial y}\bigg|_{y=0}=\frac{t_p^-\big|_{y=0}}{F}i_{\text{app}}(t) \tag{19a}$$

$$D_p^{\text{eff}}\frac{\partial c_p(y,t)}{\partial y}\bigg|_{y=L_p}=-\frac{t_p^+\big|_{y=L_p}}{F}i_{\text{app}}(t) \tag{19b}$$

where $t_p^+:=D_p^+/(D_p^++D_p^-)$ is the transference number of the positive electrode and $t_p^-=1-t_p^+$.

Note that D_p^+, D_p^-, D_p^{eff}, t_p^+, and t_p^- are all concentration-dependent and nonuniform in the positive electrode domain. This fact makes the derivation of the transfer function between the electrode concentration and the current difficult due to the complex nonlinear dependence of the parameters on the concentration. Here, we assume the values of these parameters are equal and constant at the two boundaries, e.g., $D_p^+\big|_{y=0}=D_p^+\big|_{y=L_p}$, $D_p^-\big|_{y=0}=D_p^-\big|_{y=L_p}$, etc. Next, based on a similar procedure as presented in Section III-A, a transcendental transfer function for (4) can be obtained, i.e.,

$$\begin{aligned}\frac{c_p(y,s)}{i_{\text{app}}(s)}=&-\frac{1}{FL_ps}-\frac{\tau_p}{FL_p}\times\\&\left(\frac{1}{\sqrt{\tau_ps}}\frac{\cosh\left((1-\frac{y}{L_p})\sqrt{\tau_ps}\right)}{\sinh\left(\sqrt{\tau_ps}\right)}-\frac{1}{\tau_ps}\right)-\\&\frac{t_p^+\tau_p}{2FL_p}\frac{1}{\frac{1}{2}\sqrt{\tau_ps}}\frac{\sinh\left(\left(\frac{2y}{L_p}-1\right)\frac{1}{2}\sqrt{\tau_ps}\right)}{\cosh\left(\frac{1}{2}\sqrt{\tau_ps}\right)}\end{aligned} \tag{20}$$

where $\tau_p=L_p^2/D_p^{\text{eff}}$ is the time constant for the diffusion process in the positive electrode. According to (6) and (7), the positions of interests are the boundaries $y=0$ and $y=L_p$. Unlike the electrolyte equation, there is no a general symmetrical relationship in the positive electrode domain, and thus the transfer functions for these two positions have to be approximated individually. The procedures are described as follows.

At the solid-solid interface ($y=0$), denoting $c_p^{\text{surf}}(t):=c_p(0,t)$, one can obtain the transfer function

$$\frac{c_p^{\text{surf}}(s)}{i_{\text{app}}(s)}=-\frac{1}{FL_ps}-\frac{\tau_p^{\text{surf}}}{FL_p}G_p^{\text{surf}}(s) \tag{21}$$

where

$$\begin{aligned}G_p^{\text{surf}}(s)=&\left(\frac{1}{\sqrt{\tau_p^{\text{surf}}s}}\frac{1}{\tanh\left(\sqrt{\tau_p^{\text{surf}}s}\right)}-\frac{1}{\tau_p^{\text{surf}}s}\right)\\&-\frac{t_p^+}{2}\frac{\tanh\left(\frac{1}{2}\sqrt{\tau_p^{\text{surf}}s}\right)}{\frac{1}{2}\sqrt{\tau_p^{\text{surf}}s}}\end{aligned} \tag{22}$$

and $\tau_p^{\text{surf}}=\tau_p\big|_{y=0}$ is the time constant at the left boundary of the positive electrode domain.

The first term on the RHS of (21) contributes to the change of bulk concentration in the positive electrode. The second term on the RHS of (21) is associated with the overpotentials caused by the nonuniform distribution of the concentration along the y-direction. We adopt a similar PFE method as described in Section III-A to reduce the transcendental transfer function $G_p^{\text{surf}}(s)$ to a rational form

$$G_p^{\text{surf}}(s)\approx\sum_{i=1}^{N_{p1}}\frac{b_{p1,i}}{\tau_p^{\text{surf}}s+a_{p1,i}}+\frac{t_p^+}{2}\sum_{i=1}^{N_{p2}}\frac{b_{p2,i}}{\tau_p^{\text{surf}}s+a_{p2,i}} \tag{23}$$

which can readily be realized as a state-space model with a diagonal system matrix, e.g.,

$$\frac{dc_p^{\text{avg}}(t)}{dt}=-\frac{1}{FL_p}i_{\text{app}}(t) \tag{24a}$$

$$\frac{d\tilde{c}_{p1,i}(t)}{dt}=-\frac{a_{p1,i}}{\tau_p^{\text{surf}}}\tilde{c}_{p1,i}(t)-\frac{b_{p1,i}}{FL_p}i_{\text{app}}(t)\quad\forall i\in\mathcal{N}_{p1} \tag{24b}$$

$$\frac{d\tilde{c}_{p2,i}(t)}{dt}=-\frac{a_{p2,i}}{\tau_p^{\text{surf}}}\tilde{c}_{p2,i}(t)-\frac{t_p^+}{2}\frac{b_{p2,i}}{FL_p}i_{\text{app}}(t)\quad\forall i\in\mathcal{N}_{p2} \tag{24c}$$

$$c_p^{\text{surf}}(t)=c_p^{\text{avg}}(t)+\sum_{i=1}^{N_{p1}}\tilde{c}_{p1,i}(t)+\sum_{i=1}^{N_{p2}}\tilde{c}_{p2,i}(t) \tag{24d}$$

where $\mathcal{N}_{p1}=\{1,\cdots,N_{p1}\}$ and $\mathcal{N}_{p2}=\{1,\cdots,N_{p2}\}$.

At the other boundary, $y=L_p$, a platinum (Pt) current collector is usually attached, and we denote $c_p^{\text{Pt}}(t):=c_p(L_p,t)$. Similarly, the corresponding approximated transfer function can be derived

$$\frac{c_p^{\text{Pt}}(s)}{i_{\text{app}}(s)}:=\frac{c_p(L_p,s)}{i_{\text{app}}(s)}=-\frac{1}{FL_ps}-\frac{\tau_p^{\text{Pt}}}{FL_p}G_p^{\text{Pt}}(s) \tag{25}$$

where

$$\begin{aligned}G_p^{\text{Pt}}(s)=&\left(\frac{1}{\sqrt{\tau_p^{\text{Pt}}s}}\frac{1}{\sinh\left(\sqrt{\tau_p^{\text{Pt}}s}\right)}-\frac{1}{\tau_p^{\text{Pt}}s}\right)\\&+\frac{t_p^+}{2}\frac{\tanh\left(\frac{1}{2}\sqrt{\tau_p^{\text{Pt}}s}\right)}{\frac{1}{2}\sqrt{\tau_p^{\text{Pt}}s}}\\\approx&\sum_{i=1}^{N_{p3}}\frac{b_{p3,i}}{\tau_p^{\text{Pt}}s+a_{p3,i}}+\frac{t_p^+}{2}\sum_{i=1}^{N_{p4}}\frac{b_{p4,i}}{\tau_p^{\text{Pt}}s+a_{p4,i}}\end{aligned} \tag{26}$$

and $\tau_p^{\text{Pt}}=\tau_p\big|_{y=L_p}$ is the time constant at the right boundary of the positive electrode.

The corresponding realization is

$$\frac{d\tilde{c}_{p3,i}(t)}{dt} = -\frac{a_{p3,i}}{\tau_p^{\text{Pt}}}\tilde{c}_{p3,i}(t) - \frac{b_{p3,i}}{FL_p}i_{\text{app}}(t) \quad \forall i \in \mathcal{N}_{p3} \tag{27a}$$

$$\frac{d\tilde{c}_{p4,i}(t)}{dt} = -\frac{a_{p4,i}}{\tau_p^{\text{Pt}}}\tilde{c}_{p4,i}(t) - \frac{t_p^+}{2}\frac{b_{p4,i}}{FL_p}i_{\text{app}}(t) \quad \forall i \in \mathcal{N}_{p4} \tag{27b}$$

$$c_p^{\text{Pt}}(t) = c_p^{\text{avg}}(t) + \sum_{i=1}^{N_{p3}}\tilde{c}_{p3,i}(t) + \sum_{i=1}^{N_{p4}}\tilde{c}_{p4,i}(t) \tag{27c}$$

where $\mathcal{N}_{p3} = \{1, \cdots, N_{p3}\}$ and $\mathcal{N}_{p4} = \{1, \cdots, N_{p4}\}$.

Applying the MM method once more, the PFE coefficients can be obtained. The PFE coefficients $a_{p1,i}$, $b_{p1,i}$, $a_{p3,i}$, and $b_{p3,i}$ up to $N_{p1} = 3$ and $N_{p3} = 3$ are given in Table II. Note that by comparing (22) and (26) with (16), we have $a_{p2,i} = a_{p4,i} = a_{e,i}$ and $b_{p2,i} = -b_{p4,i} = -b_{e,i}$.

TABLE II
PFE COEFFICIENTS FOR THE POSITIVE ELECTRODE DIFFUSION EQUATION

	$a_{p1,1}$	$b_{p1,1}$	$a_{p1,2}$	$b_{p1,2}$	$a_{p1,3}$	$b_{p1,3}$
$N_{p1} = 1$	15	5	–	–	–	–
$N_{p1} = 2$	9.94	2.07	95.06	11.93	–	–
$N_{p1} = 3$	9.87	2	41.98	2.6	326.15	22.4
	$a_{p3,1}$	$b_{p3,1}$	$a_{p3,2}$	$b_{p3,2}$	$a_{p3,3}$	$b_{p3,3}$
$N_{p3} = 1$	8.57	–1.43	–	–	–	–
$N_{p3} = 2$	9.9	–2.026	30.50	1.163	–	–
$N_{p3} = 3$	9.87	–2	41.2	2.68	59.08	–1.718

C. Simplified Positive Electrode Diffusion Equation Under Concentration-Dependent Diffusion Coefficients

Note that the results obtained in Section III-B are only valid under the assumptions of uniform and constant parameters. However, in practice the nonuniformity and the dependence on concentration can be significant, especially under high-rate charging/discharging conditions, the results based on the approximate transfer equation (20) can lead to a considerable accumulated error over time. Here, we introduce a factor λ to correct the time constant τ_p^{surf} in (24), i.e.,

$$\tau_p^{\text{surf*}} = \lambda\tau_p^{\text{surf}} = \left(\frac{D_p^+\big|_{y=0}}{D_p^+\big|_{y=L_p}}\right)^k \tau_p^{\text{surf}} \tag{28}$$

where k is a correction coefficient tuned by trial-and-error. It can be seen that λ equals 1 either when the diffusion coefficients are uniform along the y direction, or when $k = 0$.

D. Simplified Mass-Transfer Overpotentials

Equations (2) and (7) share the same form and they contain integrals. Thus, it is not straightforward to solve them by standard ODE solvers, and a specific numerical integration method should be used [11], which increases the complexity of the model. To avoid this, we derive and use the following simplified expressions of the mass-transfer overpotentials, given by

$$\begin{aligned}\eta_e^{\text{mt}}(t) =& \frac{2RTt_e^-}{F}\ln\left(\frac{c_e^{\text{surf}}(t)}{2c_{e0} - c_e^{\text{surf}}(t)}\right) + i_{\text{app}}(t)R_e^{\text{avg}} \\ :=& h_2(c_e^{\text{surf}}(t)) + i_{\text{app}}(t)R_e^{\text{avg}}\end{aligned} \tag{29}$$

$$\begin{aligned}\eta_p^{\text{mt}}(t) =& \frac{2RTt_p^-}{F}\ln\left(\frac{c_p^{\text{Pt}}(t)}{c_p^{\text{surf}}(t)}\right) + i_{\text{app}}(t)R_p^{\text{avg}} \\ :=& h_3(c_p^{\text{surf}}(t), c_p^{\text{Pt}}(t)) + i_{\text{app}}(t)R_p^{\text{avg}}\end{aligned} \tag{30}$$

where $R_e^{\text{avg}} = L_e/[(D_e^+ + D_e^-)\left(\frac{F^2}{RT}\right)c_{e0}]$ and $R_p^{\text{avg}} = L_p/[(D_p^+ + D_p^-)\left(\frac{F^2}{RT}\right)c_p^{\text{avg}}]$ are the volume-averaged area specific resistances for the electrolyte and the positive electrode, respectively. In both of the above equations, the two terms on the RHS are associated with ionic diffusion and ionic migration, respectively. The detail of the derivation procedure is given in Appendix.

IV. ILLUSTRATIVE EXAMPLES

The PDE model (1)–(10) of ASSBs has been experimentally validated in previous works, e.g. [8], [13]. Hence, this PDE-based model will be used as a benchmark for verification of the proposed ROM. The benchmark was simulated using the FVM, which is similar to the method described in [15] and both the electrolyte and the electrode domains were spatially discretized into 100 control volumes for high-fidelity simulation. All the models, including the benchmark and the developed PFE ROMs, were implemented in MATLAB R2016b, discretized in the time domain with a sample time of 1 s. The correction coefficient in (28) of the proposed model is set to $k = 0.31$ by trial-and-error. The parameters correspond to an ASSB cell with a capacity of 0.7 mAh, and the active material of the positive electrode is $LiCoO_2$. For this electrode, three nonlinear functions, including the equilibrium potential curve $h_1(\cdot)$ in (6) and two diffusion coefficient curves ($f_{D+}(\cdot)$ and $f_{D-}(\cdot)$) are required for simulation and they are fitted using the experimental results from [13] (See Fig. 2).

Fig. 3 shows a comparison of the results from different models, including the benchmark PDE model, the proposed PFE model with and without the correction, as well as a ROM in [11], for a 1C constant current discharge. In [11], Padé approximation is applied to the diffusion equations, polynomial approximation is applied for the migration equations, and the diffusion coefficients are all considered constant. The simulated cells were initially fully charged at 4.2 V and discharge was stopped at 3.0 V. It can be observed in Fig. 3 that the proposed PFE model compares favorably to that of the PDE model implementation. As seen in Fig. 3(d), the reduction in diffusion coefficient is precisely captured, and this results in accurate prediction of the voltage, surface concentration, as well as the migration overpotential in Fig. 3(a) to Fig. 3(c). On the contrary, when there is no correction (i.e, $k = 0$), there is an accumulated error in the diffusion coefficient, and the faster drop at the end of discharge leads to a considerable prediction error for

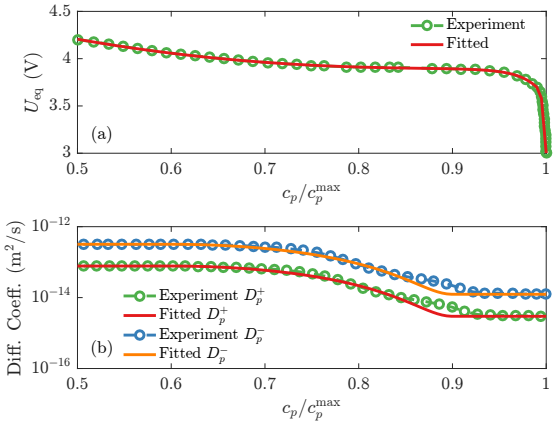

Fig. 2. Experimental and fitted curves of (a) equilibrium potential and (b) diffusion coefficients of the positive electrode.

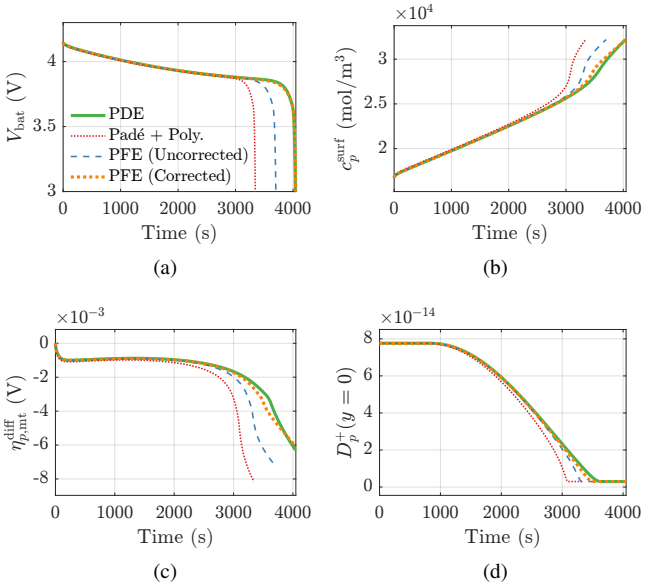

Fig. 3. Simulation results under 1C constant current discharge profile. (a) Voltage. (b) Surface concentration at $y = 0$. (c) Mass-transfer diffusion overpotential in the positive electrode. (d) Diffusion coefficient.

the knee point as seen in Fig. 3(a): The end of discharge is 283 s earlier than the benchmark PDE model. The ROM based on the method from [11] exhibits even larger errors due to its ignorance of the effect of ionic migration in the positive electrode, i.e., the migration overpotential $\eta_p^{\rm mt}$ in (30) is set to zero in [11].

Fig. 4 shows similar comparisons as given in Fig. 3, except that a 4C constant current discharge rate was applied. In this instance, the voltage error increases for all ROMs. Nevertheless, the performance of the proposed model still compares favorably to the PDE model, as the overall RMSE is only 0.18%. Indeed, at a higher current rate, the simulated error increases, while the accuracy of the corrected PFE model is still much improved than both the uncorrected PFE model and the ROM in [11].

Fig. 5 compares the PFE methods of different orders with

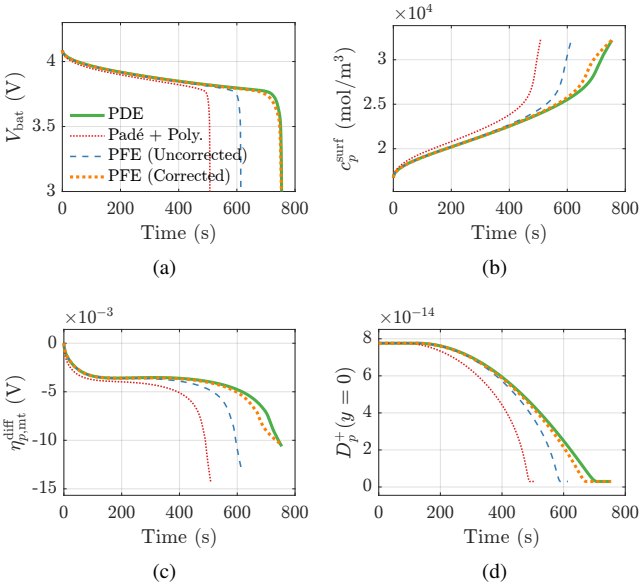

Fig. 4. Simulation results under 4C constant current discharge profile. (a) Voltage. (b) Surface concentration at $y = 0$. (c) Mass-transfer diffusion overpotential in the positive electrode. (d) Diffusion coefficient.

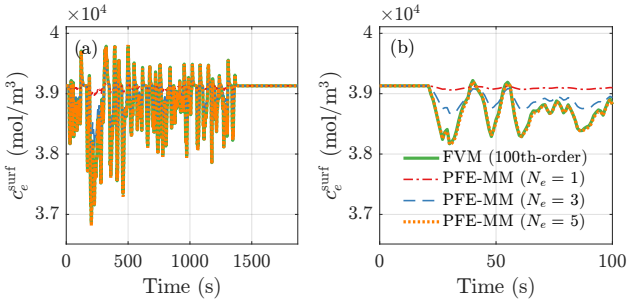

Fig. 5. Simulation results under a modified FUDS current profile: (a) Time-domain response of electrolyte concentration at $x = L_e$. (b) Details in the first 100 s.

the FVM method for the electrolyte diffusion equation under a modified Federal Urban Driving Schedule (FUDS) with the current magnitude being 4C. Clearly, the accuracy of the electrolyte can be improved by increasing the system order. In this case, it requires a fifth-order approximation to achieve high accuracy based on the proposed algorithm.

V. Conclusions

In this work, a model simplification framework is established to reduce a physics-based PDE model of ASSBs to an ODE model. The specific contributions include: 1) a generic method for ASSB model simplification for control system design; 2) Important nonlinear phenomena under high rate operation, including the concentration-dependent diffusion and the ionic migration processes in the positive electrode, are properly addressed. The derived reduced-order models can readily be implemented for online battery management functionalities such as state estimation, parameter identification, and optimal control.

APPENDIX

First, we rewrite the governing equation (3) of the electric field E_e in electrolyte as

$$\frac{\partial \Phi_e(x,t)}{\partial x} = -E_e(x,t) = \frac{1}{\kappa_e^{\text{eff}}(x,t)} i_{\text{app}} + \frac{\partial U_e(x,t)}{\partial x} \quad (31)$$

where Φ_e is the electrolyte potential, U_e is a voltage term, and κ_e^{eff} represents the local conductivity in the solid electrolyte. U_e and κ_e^{eff} are given by

$$U_e(x,t) = \frac{RT(1-2t_e^+)}{F} \ln\left(\frac{c_e(x,t)}{c_{e0}}\right) \quad (32)$$

$$\kappa_e^{\text{eff}}(x,t) = \left(D_e^+ + D_e^-\right)\left(\frac{F^2}{RT}\right) c_e(x,t) \quad (33)$$

where $t_e^+ = D_e^+/(D_e^+ + D_e^-)$ is the transference number.

Evaluating the integral of (31) over $[0, L_e]$, we have

$$\begin{aligned} -\int_0^{L_e} E_e(x,t)dx &= \Phi_e(L_e,t) - \Phi_e(0,t) \\ &= i_{\text{app}}(t)\int_0^{L_e} \frac{1}{\kappa_e^{\text{eff}}(x,t)}dx + U_e(L_e,t) - U_e(0,t). \end{aligned} \quad (34)$$

Substituting (34) into (2) yields

$$\begin{aligned} \eta_e^{\text{mt}}(t) = &\frac{RT}{F}\ln\left(\frac{c_e(L_e,t)}{c_e(0,t)}\right) + i_{\text{app}}(t)\int_0^{L_e}\left(\frac{1}{\kappa_e^{\text{eff}}(x,t)}\right)dx + \\ &+ U_e(L_e,t) - U_e(0,t). \end{aligned} \quad (35)$$

Next, we define the volume-averaged electrolyte resistance

$$R_e^{\text{avg}} := \int_0^{L_e}\left(\frac{1}{\kappa_e^{\text{eff}}(x,t)}\right)dx \approx \frac{L_e}{\bar{\kappa}_e^{\text{eff}}} \quad (36)$$

where $\bar{\kappa}_e^{\text{eff}} := \left(D_e^+ + D_e^-\right)\left(\frac{F^2}{RT}\right)c_{e0}$ is the approximated volume-averaged electrolyte conductivity.

Finally, substituting (36) and (32) into (35), and considering $t_e^- = 1 - t_e^+$, $c_e(L_e,t) = c_e^{\text{surf}}(t)$, and $c_e(0,t) = 2c_{e0} - c_e^{\text{surf}}(t)$, the expression of the mass-transfer overpotential (29) is obtained. Based on a similar procedure, (30) can be derived from (7) for the positive electrode.

REFERENCES

[1] P. Albertus, S. Babinec, S. Litzelman, and A. Newman, "Status and challenges in enabling the lithium metal electrode for high-energy and low-cost rechargeable batteries," *Nature Energy*, vol. 3, no. 1, pp. 16–21, Jan. 2018.

[2] A. C. Luntz, J. Voss, and K. Reuter, "Interfacial challenges in solid-state Li ion batteries," *J. Phys. Chem. Lett.*, vol. 6, no. 22, pp. 4599–4604, Nov. 2015.

[3] S. Randau, D. A. Weber, O. Kötz, R. Koerver, P. Braun, A. Weber, E. Ivers-Tiffée, T. Adermann, J. Kulisch, W. G. Zeier, F. H. Richter, and J. Janek, "Benchmarking the performance of all-solid-state lithium batteries," *Nature Energy*, vol. 5, no. 3, pp. 259–270, Mar. 2020.

[4] Y. Li, D. Karunathilake, D. M. Vilathgamuwa, Y. Mishra, T. W. Farrell, S. S. Choi, and C. Zou, "Model order reduction techniques for physics-based lithium-ion battery management: A survey," *IEEE Ind. Electron. Mag.*, 2021.

[5] Y. Li, M. Vilathgamuwa, S. S. Choi, T. W. Farrell, N. T. Tran, and J. Teague, "Development of a degradation-conscious physics-based lithium-ion battery model for use in power system planning studies," *Appl. Energy*, vol. 248, pp. 512–525, Aug. 2019.

[6] N. T. Tran, M. Vilathgamuwa, T. Farrell, S. S. Choi, and Y. Li, "A computationally efficient coupled electrochemical-thermal model for large format cylindrical lithium ion batteries," *J. Electrochem. Soc.*, vol. 166, no. 13, pp. A3059–A3071, Sep. 2019.

[7] K. Becker-Steinberger, S. Funken, M. Landstorfer, and K. Urban, "A mathematical model for all solid-state lithium-ion batteries," *ECS Trans.*, vol. 25, no. 36, pp. 285–296, Apr. 2010.

[8] D. Danilov, R. A. Niessen, and P. H. Notten, "Modeling all-solid-state Li-ion batteries," *J. Electrochem. Soc.*, vol. 158, no. 3, pp. A215–A222, Mar. 2011.

[9] N. Kazemi, D. L. Danilov, L. Haverkate, N. J. Dudney, S. Unnikrishnan, and P. H. L. Notten, "Modeling of all-solid-state thin-film Li-ion batteries: Accuracy improvement," *Solid State Ionics*, vol. 334, pp. 111–116, Jul. 2019.

[10] Y. Kim, X. Lin, A. Abbasalinejad, S. U. Kim, and S. H. Chung, "On state estimation of all solid-state batteries," *Electrochim. Acta*, vol. 317, pp. 663–672, Sep. 2019.

[11] Z. Deng, X. Hu, X. Lin, L. Xu, J. Li, and W. Guo, "A reduced-order electrochemical model for all-solid-state batteries," *IEEE Trans. Transport. Electrific.*, vol. 7, pp. 464–473, Jun. 2021.

[12] Z. Deng, X. Hu, X. Lin, Y. Kim, and J. Li, "Sensitivity analysis and joint estimation of parameters and states for all-solid-state batteries," *IEEE Trans. Transport. Electrific.*, vol. 7, no. 3, pp. 1314–1323, Sep. 2021.

[13] L. H. J. Raijmakers, D. L. Danilov, R. A. Eichel, and P. H. L. Notten, "An advanced all-solid-state Li-ion battery model," *Electrochim. Acta*, vol. 330, p. 135147, Jan. 2020.

[14] A. C. Antoulas, "Approximation of large-scale dynamical systems: An overview," *IFAC Proc. Vol.*, vol. 37, no. 11, pp. 19–28, Jul. 2004.

[15] Y. Li, M. Vilathgamuwa, T. Farrell, S. S. Choi, N. T. Tran, and J. Teague, "A physics-based distributed-parameter equivalent circuit model for lithium-ion batteries," *Electrochim. Acta*, vol. 299, pp. 451–469, Mar. 2019.